# Microwave Interferometric System for GPR Positioning

electronics

MDPI

*Article*

# Microwave Interferometric System for GPR Positioning

**Lapo Miccinesi *, Massimiliano Pieraccini and Chiara Lepri**

Department of Information Engineering, University of Florence, Via di Santa Marta, 350139 Firenze, Italy; massimiliano.pieraccini@unifi.it (M.P.); chiara.lepri3@stud.unifi.it (C.L.)
* Correspondence: lapo.miccinesi@unifi.it

**Abstract:** Ground penetrating radar (GPR) systems are sensors that are able to acquire underground images by scanning the surface of the soil/pavement under investigation. Usually, a GPR system records its own position along the scan line, using a mechanical odometer, i.e., a rolling wheel in contact with the ground. This simple and cheap solution can be ineffective on uneven terrains. In this paper, a positioning system based on an interferometric radar is presented. This kind of radar is able to detect small displacements of the targets in its field of view. Such a capability was used to track the GPR position along a line. The system was validated with simulations and tested in a realistic experimental scenario.

**Keywords:** Doppler effect; ground penetrating radar; global positioning system interferometric radar; radar positioning

**Citation:** Miccinesi, L.; Pieraccini, M.; Lepri, C. Microwave Interferometric System for GPR Positioning. *Electronics* **2021**, *10*, 2799. https://doi.org/10.3390/electronics10222799

Academic Editor: Peng Chen

Received: 18 October 2021
Accepted: 15 November 2021
Published: 15 November 2021



## 1. Introduction

Ground penetrating radar (GPR) systems are widely used for investigating the ground up to 2–3 m in depth [1,2]. Typically, a GPR scans a surface and records its own position along the scan line, using a mechanical odometer, i.e., a rolling wheel in contact with the ground. This is a simple and effective solution for asphalted or paved surfaces. Nevertheless, for many applications, this simple solution cannot be used.

Most of today's GPR instruments are equipped with standard global navigation satellite system (GNSS) devices [3,4]. The data loggers combine the GPR and the GNSS data during the acquisition. This is a common practice in geological surveys [5] and in archaeological prospections [6]. The main limitation of GNSS is its poor accuracy (5–6 m in the horizonal plane) [7]. Moreover, any GNSS device has serious problems of coverage in many areas and in indoor spaces. A laser theodolite tracking the GPR is another possible solution that has been tested [8]. A rotary laser system imitating the GPS on small scale has been also proposed as a positioning system for a GPR operating over rough terrains [3]. Recently, a GPR system able to retrieve its own position using an interferometric approach applied to the GPR data was proposed [9]. The main drawback of this system is that the distance, that is able to retrieve, has to be within the maximum targets' depth and the unambiguous range of the GPR. Moreover, it requires the installation of one or a couple of corner reflectors in front of the GPR.

In this paper, a positioning method based on an external interferometric microwave system is proposed that is able to track the GPR movement along a line. The same working principle can be generalized to the case of two or more radars in order to measure the three-dimensional position of the GPR.

## 2. Materials and Methods

Figure 1 shows a sketch of the proposed system. The GPR is moving with a speed $v$ toward the interferometric radar. Generally speaking, a radar is affected by the Doppler

effect, and it may not be able to retrieve the correct GPR position just by detecting the position of the peak in range [10,11].

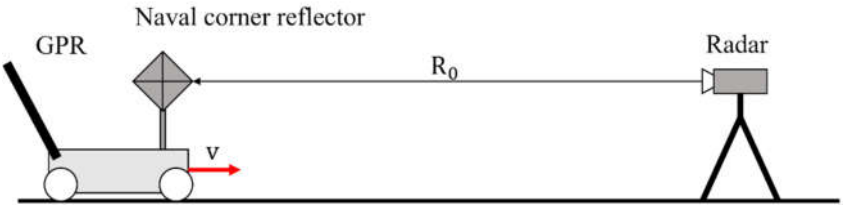


**Figure 1.** Working principle of microwave interferometric system for GPR positioning.

In order to evaluate how much the Doppler affects the interferometric radar positioning, we consider a radar providing a continuous wave stepped frequency signal, as shown in Figure 2.

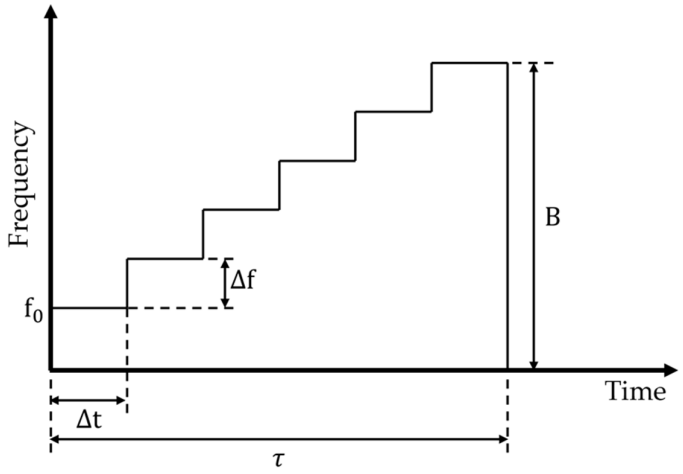


**Figure 2.** Example of continuous wave stepped frequency (CWSF) signal.

The target is assumed to be stationary during each tone; $R_0$ is the range (the distance between radar and target) at the start of the sweep. The range during the sweep is given by the following:

$$R = R_0 + nv\Delta t = R_0 + nv\frac{\tau}{B}\Delta f \quad (1)$$

with $\Delta t$ being the time duration of each single tone, $\Delta f$ the frequency increment between two subsequent tones, $\tau$ the sweep duration, and B the bandwidth.

The echo signal received at the n-frequency is as follows:

$$E_n = E_0 e^{-j\frac{4\pi}{c}(f_0+n\Delta f)\cdot R} \quad (2)$$

where $E_0$ is the amplitude of the received signal, c is the speed of light, and $f_0$ is the initial frequency.

Equation (2) can be rewritten using (1) as follows:

$$E_n = E_0 e^{-j\frac{4\pi}{c}(f_0+n\Delta f)\cdot\left(R_0+f_0\frac{v\tau}{B}\right)} e^{j\frac{4\pi}{c}f_0^2\frac{v\tau}{B}} e^{-j\frac{4\pi}{c}n^2\Delta f^2\frac{v\tau}{B}} \quad (3)$$

The last term can be neglected if $v/c \ll 1$.

The radar image can be obtained by calculating the inverse Fourier transform of the echo as follows:

$$I(R) = \sum_{n=1}^{N_f} E_n \cdot e^{j\frac{4\pi}{c}(f_0 + n\Delta f)R} \tag{4}$$

By computing the summation in (4), the radar image becomes the following:

$$I(R) \cong e^{-j\frac{4\pi}{c}f_c(R_0 - R)}\, A_N(x) e^{-j\,4\pi\frac{v\tau}{\lambda}} \tag{5}$$

with $A_N(x)$ and x:

$$A_N(x) = \frac{\sin\left(N\frac{x}{2}\right)}{\sin\left(\frac{x}{2}\right)}$$
$$x = \frac{4\pi}{c}\Delta f\left(R_0 + nv\frac{\tau}{B}f_0\right) \tag{6}$$

The Doppler effect shifts the peak position of $\Delta R_{Doppler} = nv\frac{\tau}{B}f_0$, but it does not affect the interferometric phase. Indeed, the interferometric phase, $\Delta\phi$, is as follows:

$$\Delta\phi(t) = \angle(I(R,t) \cdot I(R,t+\delta t)^*) \tag{7}$$

with $\delta t$ being the time increment, and $\angle$ the phase of a complex number. The phase in (7) is not affected by the Doppler effect if the speed is constant or if the acceleration is lower than $\lambda/\tau^2$:

$$\Delta\phi(t) = \Delta\phi_{motion} + \angle\left(e^{-j\,4\pi\frac{v\tau}{\lambda}} \cdot e^{j\,4\pi\frac{(v+\Delta v)\tau}{\lambda}}\right) = \Delta\phi_{motion} + \angle\left(e^{j\,4\pi\frac{\Delta v\,\tau}{\lambda}}\right) \tag{8}$$

where $\Delta\phi_{motion}$ is the interferometric phase related to the GPR motion, and $\Delta v$ is a possible speed increment. The condition for neglecting the second term in Equation (8) is $\left|\frac{\Delta v\tau}{\lambda}\right| \ll 1$, that is, $\left|\frac{\Delta v}{\tau}\right| \ll \frac{\lambda}{\tau^2}$.

Using realistic radar parameters, the acceleration has to be smaller than ~160 g (gravitational acceleration). This condition is surely verified in practical cases.

We would like to draw the reader's attention to this non-trivial and rather surprising statement: the Doppler effect produces a shift of the peak (using a linear frequency sweep), but does not affect the interferometry, which is able to detect the displacement without any special correction.

Indeed, with reference to Figure 3, the movement of GPR can be retrieved using the following:

$$\Delta\phi_i = \phi_{i+1} - \phi_i = \frac{4\pi}{\lambda}\Delta R \tag{9}$$

with $\lambda$ being the wavelength. $\Delta R$ must be smaller than $\lambda/4$ to avoid phase wrapping.

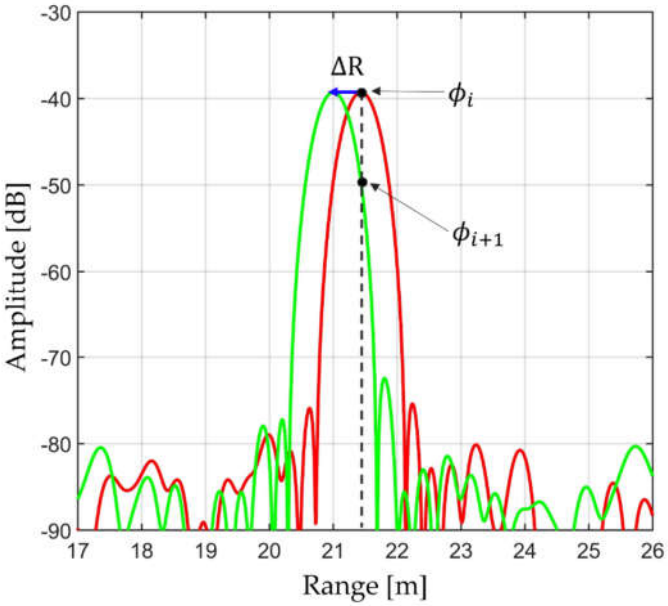


**Figure 3.** Interferometric method for GPR positioning.

Finally, the k-position of GPR can be retrieved using the position of first peak (by supposing that the initial speed of GPR is zero):

$$R_k = R_0 + \Delta\phi_i \frac{\lambda}{4\pi} \cdot k \tag{10}$$

## 3. Results

### *3.1. Simulations*

The method was tested with simulations considering the configuration in Figure 1 and the echo in Equation (2). The radar image was obtained by calculating the IFFT (inverse fast Fourier transform) of the echo. The echo was windowed (in frequency domain) using a Kaiser window with $\beta = 5$. The initial frequency was $17\ \mathrm{GHz}$, the bandwidth was $400\ \mathrm{MHz}$, the number of tones was 2666, and the tone interval was $1.01\ \mu\mathrm{s}$ (so the sweep time was $2.70\ \mathrm{ms}$). A Gaussian noise (15 dB) was added to the echo.

An example of simulation is shown in Figure 4. The GPR moved at a constant speed of $1.6\ \mathrm{m/s}$ (the maximum allowed by the phase wrapping). The yellow signal corresponds to the peak of GPR. The nominal Doppler shift was about $-184\ \mathrm{mm}$.

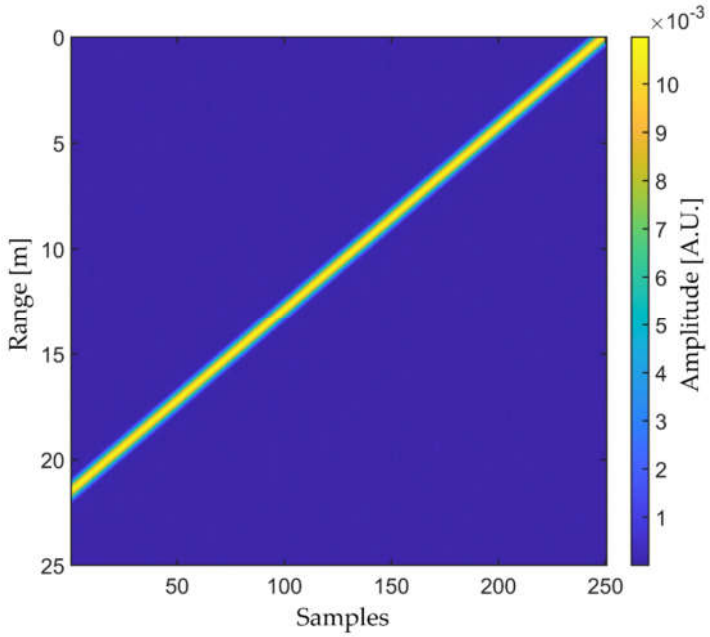


**Figure 4.** Radar image of GPR with speed of 1.6 m/s.

Figure 5a shows the position retrieved by interferometry using Equation (8) (red line) and detecting the peak position (green line). Figure 5b shows the difference between the nominal position and the position retrieved by the radar. The average difference between the interferometric position and the nominal value was about 2.95 µm for the peak −172 mm. This value is a bit different from the nominal value −182 mm. We observed that this discrepancy depends on the padding factor, which in this specific was 50. Higher values give better agreement.

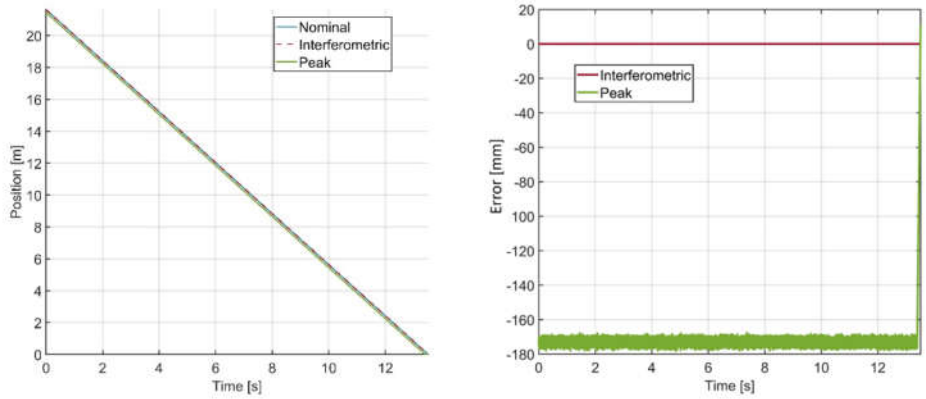


(**a**) (**b**)

**Figure 5.** Position retrieved by radar: (**a**) using the interferometric method (green line) and using the peak position (red line); (**b**) error with respect to the nominal position.

Two more realistic speed profiles were considered. In Figure 6, we suppose that the GPR was moving at a constant speed of 1.6 m/s along the path, but was stationary both at the beginning and at the end of the path. The acceleration and deceleration were about $1.5 \times 10^6$ m/s$^2$ (six orders more than the condition in (8)). We observe that the interferometric error was constant during the path at a constant speed (Figure 6b), but the acceleration generated an offset of about 3 mm.

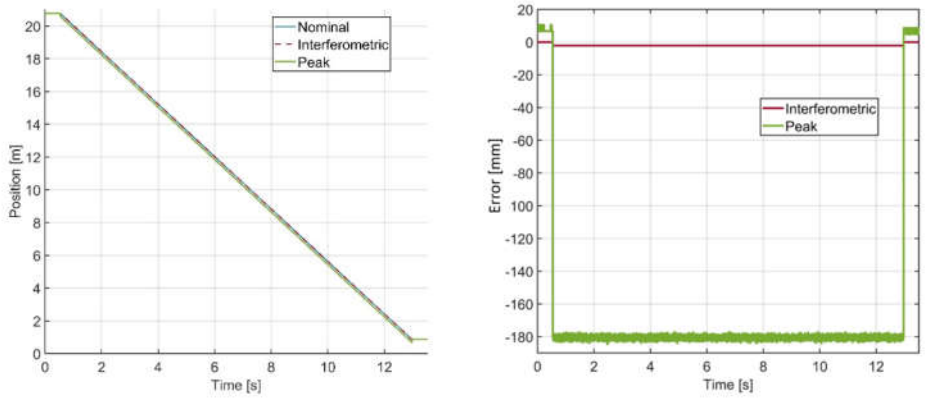


(**a**) (**b**)

**Figure 6.** Position retrieved by radar: (**a**) using the interferometric method (green line) and using the peak position (red line); (**b**) error respect to the nominal position.

Finally, Figure 7 shows an example of the sinusoidal profile. The maximum speed was 1.6 m/s and the maximum acceleration was $0.6\ m/s^2$ ($\sim 0.06$ g). Figure 7b shows the measurement error that is zero when the speed is almost zero and maximum when the acceleration is at its highest value (t = 4 s). The maximum error was 2.17 mm. It is due to the Doppler effect contribution that is not completely negligible when the acceleration is not zero.

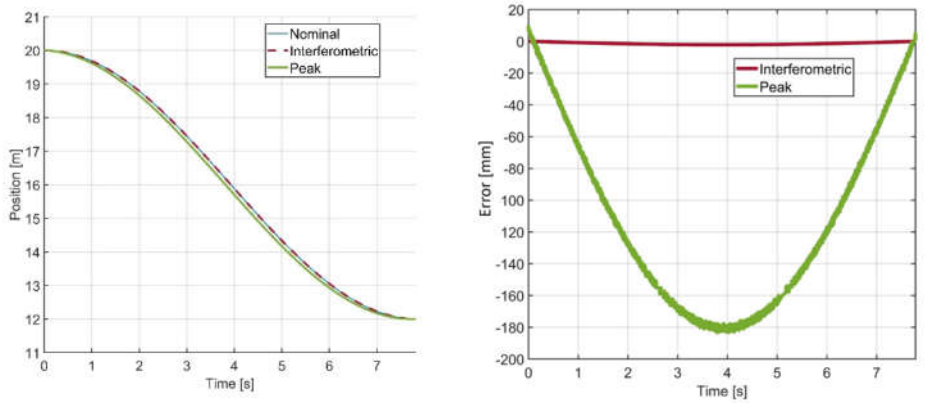


(**a**) (**b**)

**Figure 7.** Position retrieved by radar: (**a**) using the interferometric method (green line) and using the peak position (red line); (**b**) error with respect to the nominal position.

### *3.2. Experimental Results*

The experimental setup is shown in Figure 8. The interferometric radar used was an IBIS radar by IDS-Georadar, Pisa Italy. The GPR system was ORFEUS, developed by the ESECH Lab within the framework of a European Project [12,13]. ORFEUS provides a CW-SF signal with 500 MHz central frequency and 1 GHz bandwidth. The number of tones of a single weep was 200. The repetition rate was about 47 Hz.


**Figure 8.** Experimental setup for GPR positioning by interferometric radar.

The interferometric radar was in front of the GPR that was moved along a straight line (presumably with an accuracy of a few cm). In order to evaluate possible drifts due to measurement errors, the GPR was moved roundtrip from the initial position to the same final position.

IBIS provides a continuous wave frequency modulated (CWFM) signal with a 17.2 GHz central frequency, 400 MHz bandwidth, and 2666 samples for each sweep (the samples are equivalent to the frequency tones in (2)). The sweep time was 2.7 ms.

Figure 9 shows the position retrieved by the interferometric radar. The GPR was moved for about 18 m straight toward the interferometric radar and back to the initial position. The system error can be evaluated using the standard deviation of the difference between the first and the last position. It was about 87 mm.

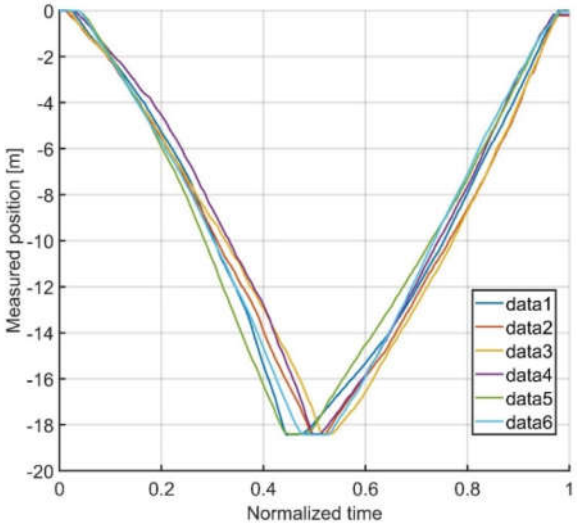


**Figure 9.** GPR position retrieved by interferometric radar.

Finally, Figure 10 shows an example of the B-scan obtained using the proposed method. The position retrieved by IBIS was synchronized and stacked with the sweeps of ORFEUS. The signals at 16 m and 26 m are related to two storm drains. No other targets are visible in the scanned area [11].

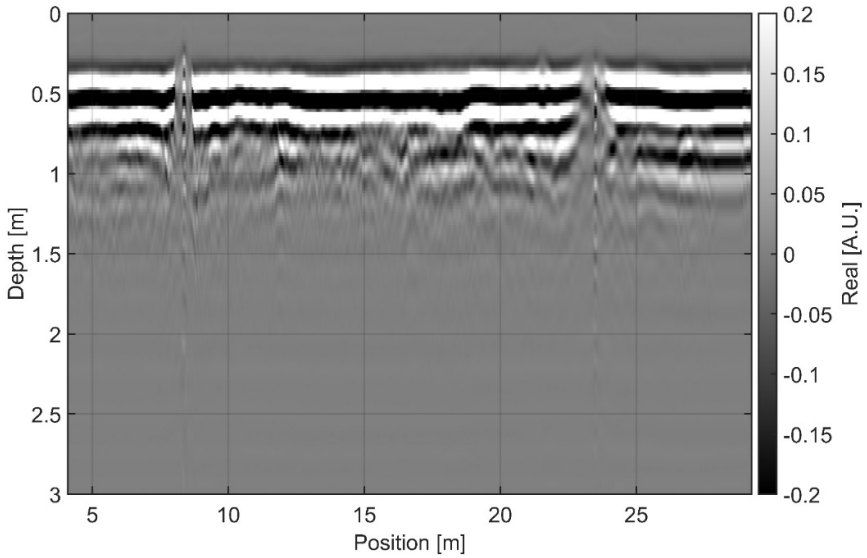


**Figure 10.** GPR signal synchronized and stacked with position retrieved by IBIS.

## 4. Discussion

A notable theoretical point demonstrated in this this article (both theoretically and experimentally) is that the Doppler effect affects the peak position of a target (the well-known "Doppler shift"), but it does not affect its phase, which, for this reason, can be used for retrieving the position of the target when its initial position is known. On the other hand, as any interferometric technique is an incremental method, it could be prone to drifts caused by the random accumulation of statistical errors. In effect, the system tested in a realistic scenario has given an experimental uncertainty of about 90 mm, traveling a path of about 40 m (meaning an error of 0.22 %). This is a drawback of this method that should be always taken into account also if it is not different from the drift to which also the odometer is subject when used for tracking lines of several meters.

## 5. Conclusions

In this paper, a GPR positioning system is proposed. The system is based on an interferometric radar that is able to detect small displacement of targets in its field of view. Its accuracy on flat terrain is comparable to the metric wheel (odometer), the most popular positioning device, with the advantage that, as the device does not need direct contact with the ground, it can operate on any terrain.

With respect to GNSS, this system is able to operate indoors and in zones without satellite coverage, but obviously it needs the deployment of special equipment that should be suitably georeferenced.

Despite the advantages above mentioned, the obvious drawback of the proposed equipment is its cost and the complexity of the in-field deployment. A cost–benefit balance has to done for any specific application. Looking ahead, the cost of RF electronics is decreasing rapidly, and therefore, this solution could become cost-effective in a few years.

Finally, although the working principle of the equipment reported in this article could potentially solve the typical problems of a GPR operating on rough terrains, we determine that for retrieving the radar position on a not-flat surface, it is necessary to have

at least two radar points of view, and possibly three, for obtaining the vertical position. Such complex equipment is out of the scope of this article.

**Author Contributions:** Conceptualization, M.P. and L.M.; methodology, L.M.; software, L.M.; validation, L.M. and M.P.; formal analysis, L.M. and C.L.; investigation, C.L.; resources, M.P.; data curation, L.M.; writing—original draft preparation, L.M.; writing—review and editing, M.P.; visualization, L.M.; supervision, L.M.; project administration, M.P.; funding acquisition, M.P. All authors have read and agreed to the published version of the manuscript.

**Funding:** This research received no external funding.

**Data Availability Statement:** Data available on request.

**Conflicts of Interest:** The authors declare no conflict of interest.

## References

1. Carrick Utsi, E. *Ground Penetrating Radar: Theory and Practice*; Butterworth-Heinemann: Oxford, UK, 2017.
2. Persico, R. *Introduction to Ground Penetrating Radar: Inverse Scattering and Data Processing*; IEEE Press Series on Electromagnetism; 2014.
3. Grasmueck, M.; Viggiano, D.A. Integration of ground-penetrating radar and laser position sensors for real-time 3-D data fusion. *IEEE Trans. Geosci. Remote. Sens.* **2007**, *45*, 130–137.
4. Manacorda, G.; Miniati, M.; Sarri, A.; Consani, M.; Penzo, A. Designing a GPR system for the snow-thickness measurement on Mounts Everest and Karakoram. In Proceedings of the Tenth International Conference on Ground Penetrating Radar, Delft, The Netherlands, 21–24 June 2004.
5. Urbini, S.; Vittuari, L.; Gandolfi, S. GPR and GPS data integration: Examples of application in Antarctica. *Ann. Geofis.* **2001**, *44*, 687–702.
6. Dimic, F.; Mušič, B.; Osredkar, R. An example of an integrated GPS and DR positioning system designed for archeological prospecting. *Inf. MIDEM* **2008**, *38*, 144–148.
7. Ferrara, V.; Pietrelli, A.; Chicarella, S.; Pajewski, L. GPR/GPS/IMU system as buried objects locator. *Measurement* **2018**, *114*, 534–541.
8. Young, R.A.; Lord, N. A hybrid laser-tracking/GPS location method allowing GPR acquisition in rugged terrain. *Lead. Edge* **2002**, *21*, 486–490.
9. Miccinesi, L.; Pieraccini, M. A GPR Able to Detect Its Own Position Using Fixed Corner Reflectors on Surface. *IEEE Trans. Geosci. Remote. Sens.* **2021**, *59*, 4725–4732.
10. Pieraccini, M.; Miccinesi, L.; Rojhani, N. A Doppler Range Compensation for Step-Frequency Continuous-Wave Radar for Detecting Small UAV. *Sensors* **2019**, *19*, 1331.
11. Pieraccini, M.; Miccinesi, L. CWSF radar for detecting small UAVs. In Proceedings of the 2017 IEEE International Conference on Microwaves, Antennas, Communications and Electronic Systems (COMCAS), Tel-Aviv, Israel, 13–15 November 2017; pp. 1–5, doi:10.1109/COMCAS.2017.8244710.
12. Parrini, F.; Pieraccini, M.; Grazzini, G.; Spinetti, A.; Macaluso, G.; De Pasquale, G.; Testa, C. ORFEUS GPR: A very large bandwidth and high dynamic range CWSF radar. In Proceedings of the XIII International Conference on Ground Penetrating Radar, Lecce, Italy, 21–25 June 2010
13. Pieraccini, M.; Miccinesi, L.; Canizares, H.G. Critical Verification of the Underground Cartography of the Municipality Using a High Performance Ground Penetrating Radar. In *Proceedings of the 10th International Workshop on Advanced Ground Penetrating Radar (IWAGPR 2019), The Hague, Netherlands, 8-12 September 2019*; M Publisher: European Association of Geoscientists & Engineers, pp. 1–6, doi:10.3997/2214-4609.201902569.